PAPER • OPEN ACCESS

Are tungsten-based nuclear fusion components truly invisible to x-ray inspection?

To cite this article: Triestino Minniti and Heather Lewtas 2022 *Nucl. Fusion* **62** 066003

OPEN ACCESS
IOP Publishing | International Atomic Energy Agency
Nuclear Fusion

Nucl. Fusion **62** (2022) 066003 (8pp)
https://doi.org/10.1088/1741-4326/ac4efe

Are tungsten-based nuclear fusion components truly invisible to x-ray inspection?

Triestino Minniti* and **Heather Lewtas**

UKAEA-United Kingdom Atomic Energy Authority, Culham Science Centre, Abingdon, OX14 3DB, United Kingdom of Great Britain and Northern Ireland

E-mail: triestino.minniti@ukaea.uk

Received 13 December 2021, revised 20 January 2022
Accepted for publication 26 January 2022
Published 30 March 2022

Abstract

The ability to detect undesired volumetric defects in reactor components could affect the safety and reliability of a fusion power plant and change the expected lifetime and performance of the reactor. This is even more true for critical reactor parts like plasma-facing components (PFCs) which have to withstand challenging in-vessel conditions due to a combination of plasma bombardment, radiation, and nuclear heating. The structural integrity of these components prior to their installation in a nuclear fusion reactor needs to be assessed non-destructively. Until now, industrial x-ray radiography and tomography have not been used to non-destructively inspect fusion components due to their lack of penetration power into dense material such as tungsten which is often used to manufacture PFCs. However, aiming to revert this consolidated belief, we have demonstrated for the first time the feasibility of assessing volumetric defects non-destructively on DEMO divertor mock-up by means of MeV energy range x-ray tomography. The authors believe that the application of this technology could be easily extended for inspecting large fusion components and positively impact procedures to be followed in the qualification of fusion components for current and future nuclear reactors.

Keywords: divertor target, tungsten, thermal break, CuCrZr, x-ray tomography, non-destructive evaluation, qualification

(Some figures may appear in colour only in the online journal)

1. Introduction

In a magnetic confinement nuclear fusion reactor plasma-facing components (PFCs) are the most exposed elements to high heat flux (HHF) loads due to a combination of plasma bombardment, radiation and nuclear heating by neutron irradiation [1]. Such neutron fluxes produce defects in the microstructure of the materials and pulsed operation of the reactor causes fatigue due to cyclic thermal stress variation [2, 3]. In fact, in the case of ITER and DEMO reactors, it is expected that the peak surface heat flux on divertor targets could reach up to 10 MWm^{-2} during normal operation and 20 MWm^{-2} during slow transient events such as loss of plasma detachment. To maintain structural integrity under HHF fatigue loads and demonstrate reliable HHF performance, PFCs need to be carefully inspected and qualified before their installation in the reactor. Any manufacturing defect in the component could quickly develop into a failure because of the detrimental in-vessel high radiation bombardment which might impact on the reliability of the entire fusion power plant. As such, robust non-destructive evaluation (NDE) techniques are paramount to avoid failures and they will represent a crucial step for qualifying fusion components to any fusion regulatory codes and standards required for a

* Author to whom any correspondence should be addressed.

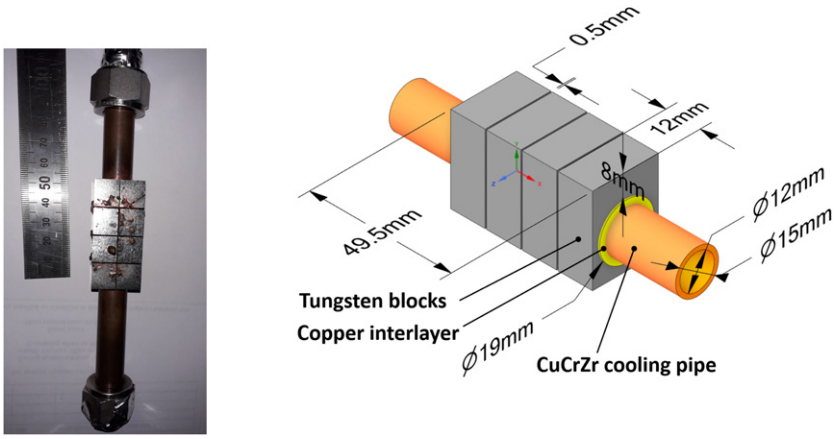

Figure 1. (Left panel) Photograph of the DEMO divertor target studied by means of 6 MeVs energy XCT. (Right panel) A schematic drawing with the relevant dimensions of the sample.

commercial fusion power plant. Very recently, we have successfully demonstrated the use of neutron tomography as a non-destructive volumetric inspection technique applied to PFCs [4]. However, such inspection technology can only be accessed at dedicated large-scale facilities limiting its applicability in practice. X-ray computed radiography and x-ray computed tomography (XCT) are very well-established technologies that are used routinely to non-destructively inspect engineering components across many industries (nuclear, aerospace, oil & gas, etc). These techniques might be considered the first option for qualifying critical engineering components where stringent quality controls are required. Until now, industrial x-ray radiography and tomography were never used to inspect fusion components due to the lack of penetration power into dense material like tungsten (W) which is often used to manufacture PFCs. In this work, we demonstrated the feasibility of using MeV energy range XCT for non-destructive inspect volumetric defects on a DEMO divertor mock-up.

2. DEMO divertor mock-up sample and previous testing

For this pilot experiment a thermal break DEMO divertor target [2, 5–7] whose features are derived from phase 2 design [8] has been used and it is shown in the left panel of figure 1. A schematic drawing with all relevant dimensions of the sample is also depicted on the right panel of the same figure. The specimen was produced by machining W to size and casting oxygen-free high conductivity (OFHC) copper (labeled as copper interlayer on the right panel of figure 1) into the bore of the block. The OFHC copper was left 2 mm proud of the W block to allow subsequent thermal break features to be machined into the interlayer. The blocks together with casting were provided by ALMT (Japan). Thermal break features were wire eroded in the interlayer [8]. Parts were precisely bored to match the outer diameter of 15.00 ± 0.01 mm CuCrZr alloy pipe. A detailed description of the mock-up manufacturing process is report in this work [8] and it has been listed in the reference for interested readers.

This sample was previously studied via neutron tomography [4] on the IMAT beamline [9–15] at the ISIS spallation neutron source in the UK. Further, recent studies have demonstrated the feasibility of using neutron tomography to assess volumetric defects on large numbers of similar components like divertor monoblocks [13] and how those results compared with XCT measurements [16]. From the neutron tomography tests [4], no major issues have been identified within the sample. Subsequently, the specimen was subjected to HHF loads with a single cycle at $\sim$8 MWm^{-2} on the HIVE facility [17] at United Kingdom Atomic Energy Authority (UKAEA). During this test, a loss of cooling flow was experienced which led to bulk boiling in the pipe-work and a subsequent expansion of the specimen in its central area. The rapid expansion led to a leak of the coolant and rapid migration of some of the inner pipe and interlayer materials to the surface of the W armour as shown in figure 1. To understand the damage created by the failure, we propose to test the feasibility of using MeV energy range XCT as a volumetric non-destructive inspection method for preserving the integrity of the sample.

3. High energy x-ray system and testing methodology

High energy x-ray radiography and tomography a MeV energy range are emerging techniques that only recently have been used to inspect very large engineering components where conventional XCT at keV energy range lacks penetration power into the sample. Hence, this technology offers a potential new route for qualifying large fusion components very often manufactured with dense materials like W or where sizes prevent the use of standard keV energy range XCT.

For this feasibility experiment, high-energy x-rays radiographs of the specimen were collected at the North Star Imaging (NSI) facility in the United States using a 6 MeV linac-based x-ray scanner [18]. A schematic of the facility is visible in figure 2(a) which includes a linac-based x-ray source, a manipulator, and the x-ray detector. The dimensions of the facility are 9.65 m $\times$ 2.79 m $\times$ 3.43 m ($L \times W \times H$) at the net of the shielding construction which is surrounding it.

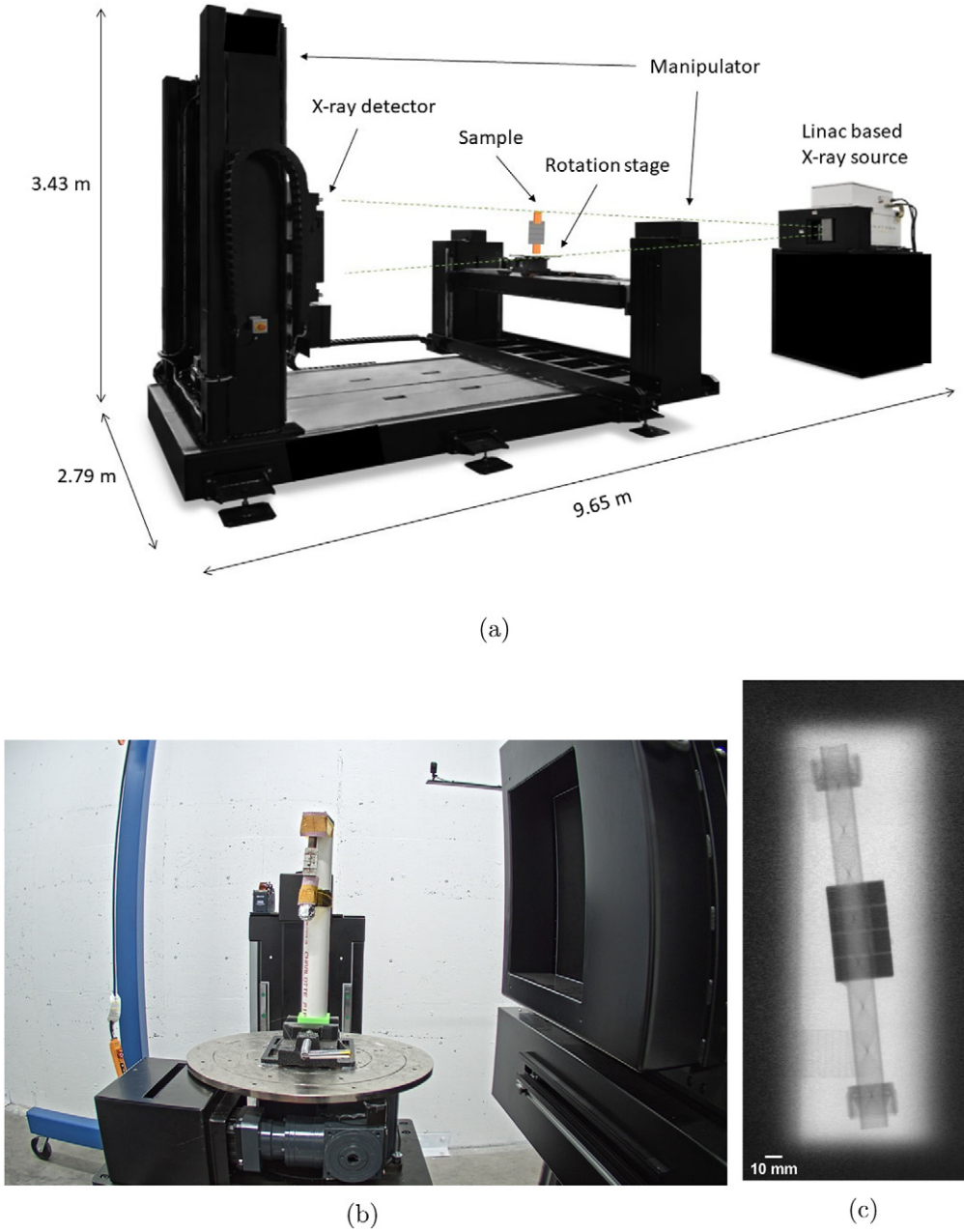

Figure 2. (*a*) A schematic of the facility which includes a linac-based x-ray source, a manipulator, and the x-ray detector. The dimensions of the facility are 9.65 m × 2.79 m × 3.43 m ($L \times W \times H$) at the net of the shielding construction which is surrounding it. The image shown is reproduced with the permission of NSI. (*b*) Detailed view of the sample setup mounted on the rotation stage of the manipulator. (*c*) Image of the sample at 0° angle as acquired in the tomography scan.

The sample was fixed on the rotating platform using a plastic tube which is weakly interacting with high-energy photons as shown in figure 2(*b*). The detection system consisted of a flat panel digital x-ray detector based on linear diode array (LDA) with 3072 × 3072 pixels and a pixel pitch of 139 μm. A cone beam geometry and a magnification of 1.107 was chosen assuring with a beam focal spot of 1.3 mm a geometrical unsharpness U_g of the specimen at the image plane of 119 μm. The tomography of the sample was collected by performing a uniformly spaced angular scan of 720 projections in the range $[0°, 360°)$ with a total acquisition time of 4 h. An image of the sample acquired at 0° angle during the tomography scan is shown in figure 2(*c*). No normalization correction has been applied to the image which has been only cropped for a better visualization. Additionally, a few images were taken for normalization purposes (three flat field and one dark field images) prior to starting the scan. The acquired projections largely satisfied by a factor of 1.7 the minimum number of required images necessary to fulfill the Nyquist–Shannon sampling theorem [19]. The computed tomography (CT) reconstruction of the sample was performed by filtered back projection (FBP) [19] using the NeuTomPy toolbox [20] software.

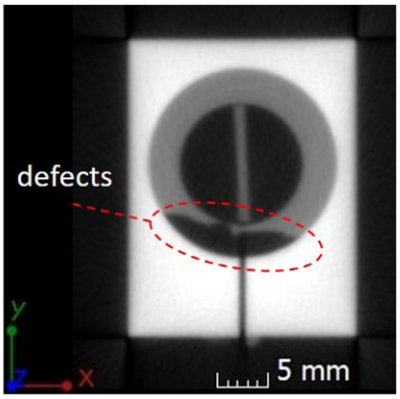

(a) X-Y cross-section view.

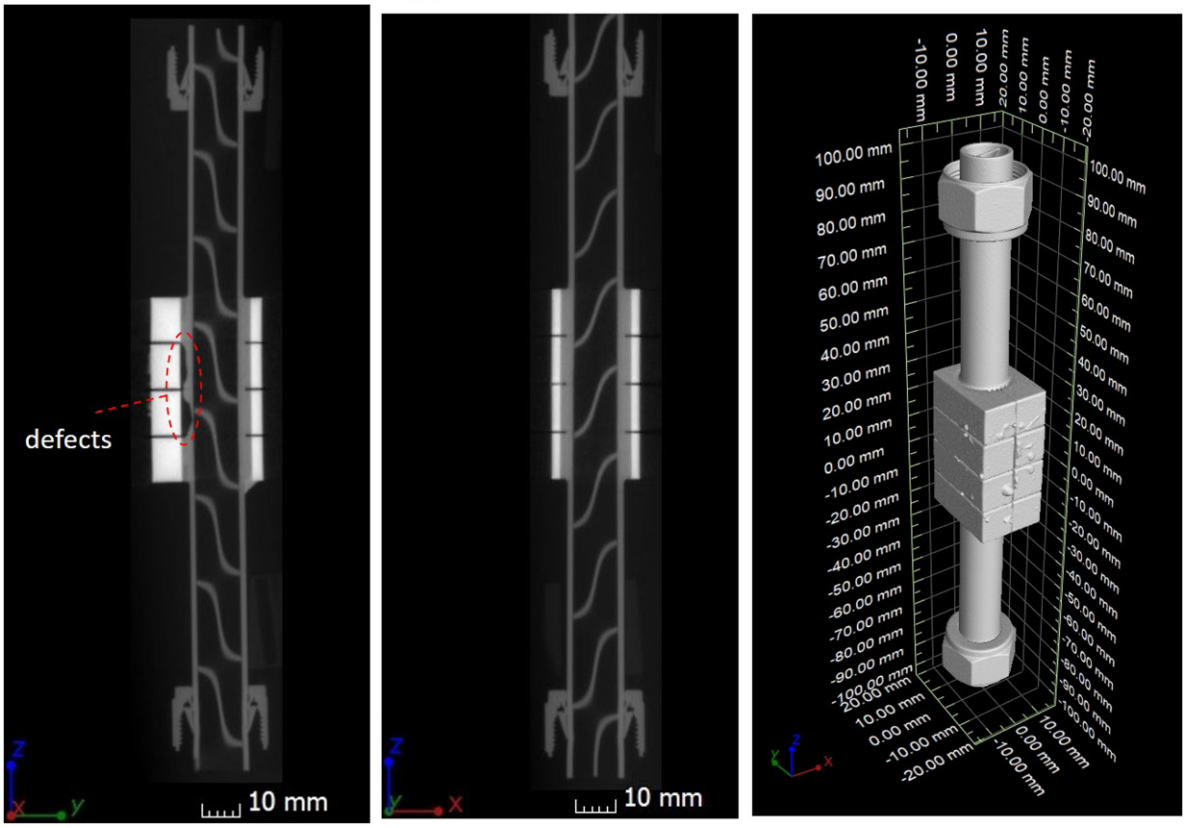

(b) Y-Z cross-section view. (c) X-Z cross-section view. (d) 3D volume rendering.

Figure 3. Cross-section views and 3D volume rendering of the DEMO divertor mock-up extracted from XCT data at MeV energy range.

4. Results and discussion

In this section, we will discuss results showing volumetric defects present in the DEMO divertor mock-up caused by the HHF test performed on the HIVE facility [17] at UKAEA. The specimen was studied non-destructively with a spatial resolution (voxel size) of 139 μm and a geometrical unsharpness of 119 μm. Smaller defect sizes with respect to the achieved spatial resolution were considered to not be distinguishable with the current experimental setup. After FBP reconstruction, some selected cross-sectional views of the specimen are reported in figures 3(a)–(c) and the full volume rendering of the object is shown in figure 3(d). From these results, damage to the component is clearly visible from the x–y and y–z cross-section images which have revealed multiple failures of the inner CuCrZr alloy pipe and the oxygen-free high conductivity (OFHC) copper interlayer. Damage to the component is particularly located in the proximity of the two central monoblocks. Melted materials caused by the HHF load have been partially deposited on the external W tile surface and they are visible in the 3D volume rendering image of the specimen in figure 3(d) as well as on the picture of the sample reported in the left panel of figure 1.

The x–y cross-section image of figure 3(a) has further revealed a complete loss of the structural integrity of the pipe in the proximity of the joints between monoblocks where the

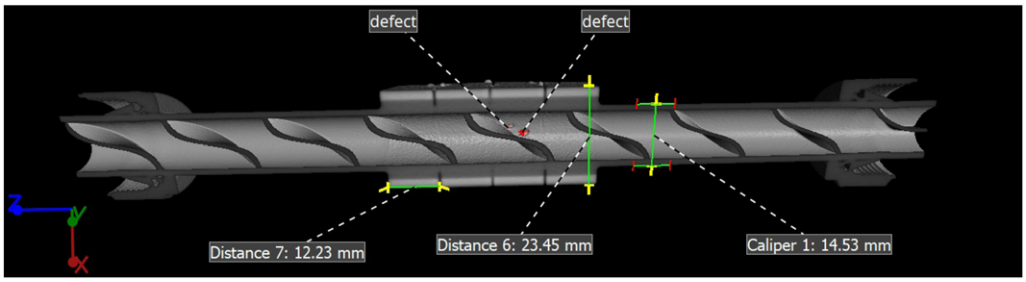

Figure 4. Volume rendering of the inner structure of the DEMO divertor mock-up where holes in the CuCrZr pipe have been highlighted ('defect' label). Metrology checks of some dimensions of the component were super-imposed as well for completeness.

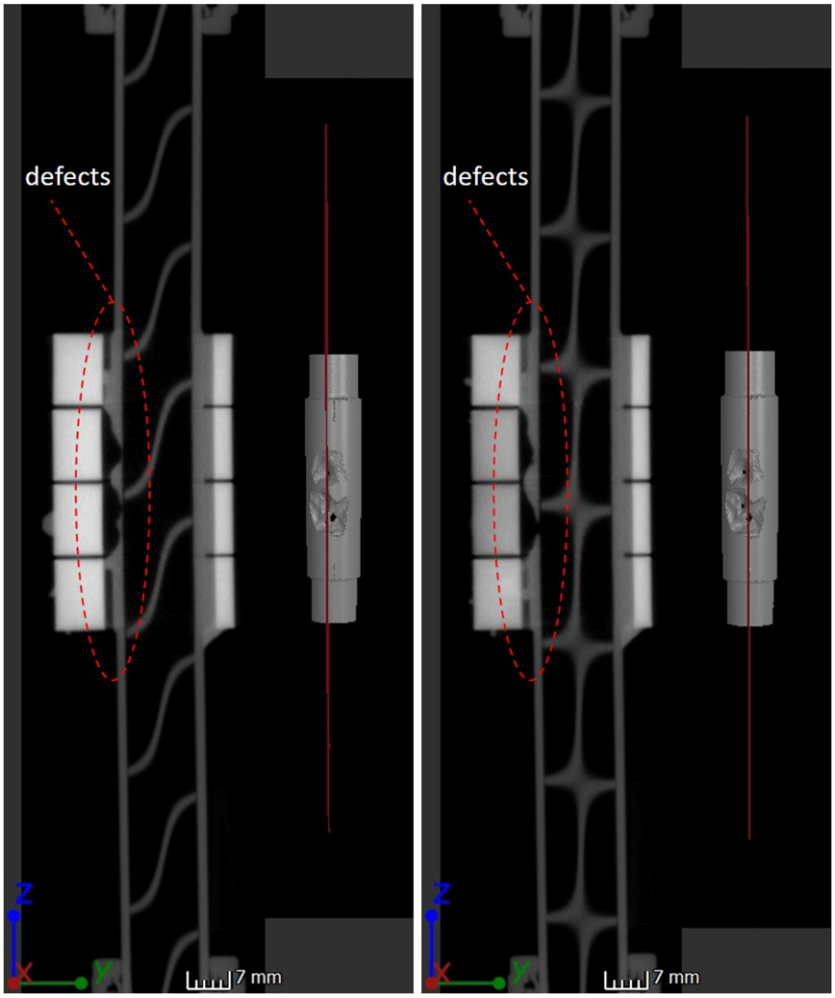

Figure 5. y–z cross-section views of the component in coincidence of the holes detected in the CuCrZr pipe. Left panel reports the first two pipe holes which are aligned vertically along the z axis, rather the third one is shown separately in the right panel of the figure. An insert displaying a 3D rendering of the component where W tiles has been masked (description provided in the main text) has been embedded in each panel for helping the reader localizing the cross-section image respect to the 3D rendering of the sample.

pressure relief after boiling has resulted in the formation of some holes in the pipe with the subsequent loss of coolant. The good spatial resolution achieved in the tomography scan is also testified by the level of detail in the reconstruction of the threads of the two pipe fittings utilised to attach the mockup to the external cooling loop during the HHF test on HIVE, and visible in the y–z and x–z cross-section images of figures 3(b) and (c). Further, in the scan we been able to resolve details of the inner structure of the divertor target mockup and the helical swirl tape that runs through the entire length of the cooling pipe as shown in the cross-section images of figures 3(b) and (c), and in the subsequent figure 4. Figure 4 shows a 3D rendering of the divertor mockup where only about half of the component has been considered, this allows us to better understand the location of some of the holes present in the CuCrZr pipe, indicated in the figure with the label named 'defect'.

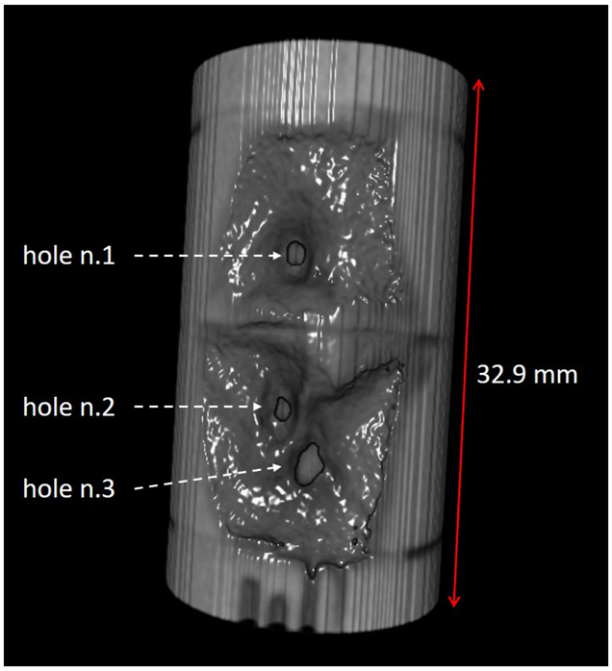

Figure 6. 3D rendering of the damage of the component caused after the HHF test performed on the HIVE facility.

Metrology of the dimensions of the pipe outer diameter, W monoblock length, and monoblock thickness have been performed and are also visible in this figure. These measurements match very well with the dimensions of the component shown in the schematic drawing presented in the right panel of figure 1.

A better representation of the damage caused by failure during HHF load of the component has been achieved via virtual removal of the W tiles of the mock-up and obtained by masking with a cylindrical region of interest aligned in the respect to the pipe axis in the volume rendering of the sample. The result of this procedure is visible in the insert image embedded in each panel of figure 5. This image shows large melting regions in the OFHC copper interlayer and holes in the CuCrZr pipe of the specimen. Cross-section views depicted in figure 5 highlight the presence of three holes in the CuCrZr pipe which as previously said, are all located in the two central monoblocks of the divertor target. Two holes are visible in the y–z cross-section shown in the left panel of figure 5 because they were vertically aligned along the z axis. The third hole in the CuCrZr pipe is then depicted in the y–z cross-section image on the right panel of the same figure.

To quantify the amount of material lost, a section of the volume close to the damage of the mock-up has been considered and shown in figure 6. This section has been obtained by extracting a sub-volume from the previous 3D rendering of the divertor target depicted in figure 5 where we hidden from the CT data the internal swirl tape volume with a similar procedure applied for masking the external W tiles discussed before. After manufacture and before any damage caused by the HHF load this selected section of the sample has a cylindrical shape with an external diameter of 19 mm if we sum the OFHC copper interlayer thickness of 4 mm to the pipe outer diameter of 15 mm, an internal CuCrZr pipe diameter of 12 mm, and a length of 32.9 mm (as deduced by figure 6). With these dimensions its estimate overall volume is 5607.193 mm^3 within the assumption of a perfect cylindrical symmetry. Instead, the analysis of this section performed by means of VGSTUDIO MAX [21] has revealed a total volume of 2463.480 $\pm$ 0.003 mm^3, i.e. a net loss of 3143.713 $\pm$ 0.003 mm^3 of melted materials which have been partially deposited on the W tile surfaces of the component (see photo of the sample in figure 1).

The quantification of the surface of each hole detected in the cooling pipe has followed a differ data analysis route because to its irregular geometrical shape, and it has been based on the idea of unrolling virtually the volume for the section of sample depicted in figure 6. The direction of unrolling is clockwise as highlighted by the blue arrow in the left panel of figure 7 which has been superimposed to a cross-section view of the analysed volume. From the resulting unrolled volume a slice close to the inner diameter of the pipe (following the dashed green line in figure 7) has been extracted and it is shown in the right panel of the same figure.

As expected, the holes in the CuCrZr pipe have an irregular shape difficult to evaluate with simple geometrical calculations. The computation of each hole dimension has required first the detection of its contour, after which the area could be evaluated knowing the pixel size. This has been done automatically by applying the 'analyze particles' plugin [22] available for the ImageJ software [23] to the unrolled slice. The contour limit of each hole area is visible in the insert of the right panel of figure 7 and drawn in the image as a solid red line. Table 1 shows the outcome of the analysis where we report the area of each pipe hole in square millimetres obtained by computing the number of pixels falling within each contour, its error set to be equal at the area of one pixel, the ellipse aspect ratio, and ellipse roundness after fitting the contour with an ellipsoidal function.

These results enable us to further predict the amount of coolant lost per second during the HHF test on the HIVE facility. In fact, during the HHF experiment the coolant flow rate was set constant at 116.67 $cm^3\ s^{-1}$ as reported in table 2.

The CuCrZr pipe used to carry the coolant has an internal diameter of 12 mm, i.e. its internal pipe area of 1.13 cm^2. The averaged flow velocity of 103.16 cm s^{-1} for the coolant has been calculated by the ratio of the coolant flow rate and the internal pipe area, as indicated in the forth column of table 2. Finally, the flow rate of coolant lost in each pipe hole was computed as the product of the coolant average flow velocity by the area of each hole and reported in the last column of the table. It can been seen from these estimated values that every second a total of about 4 cm^3 of coolant has been lost thorough the pipe holes and deposited into the vacuum chamber hosting the HHF test on HIVE. Those estimated values for the loss of coolant through the detected pipe holes have not yet been verified experimentally by independent measurements, and further investigations in this direction on the sample will be planned in the future.

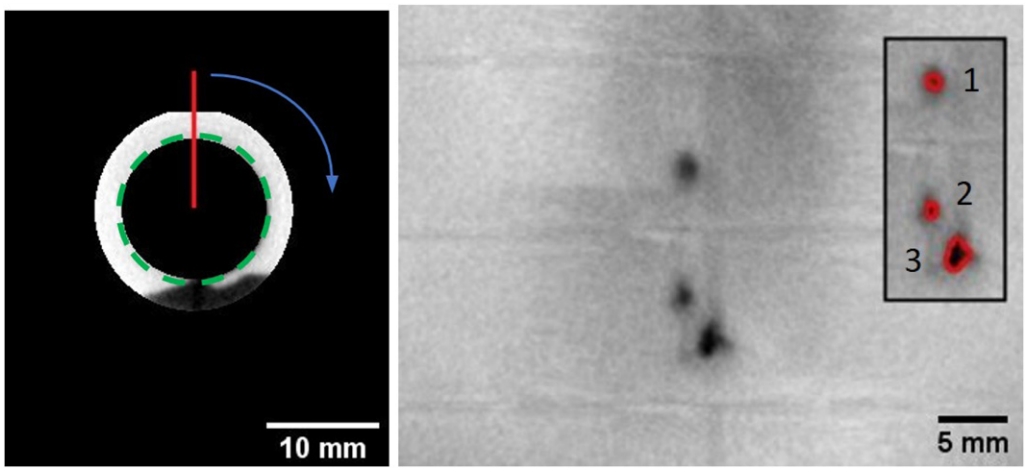

Figure 7. (Left panel) Virtual unrolling direction of the analysed CT volume for the section of component in figure 6 together with the indication where the slice from the unrolled volume has been taken, and reported as a dash green line in the image. (Right panel) Slice of the unrolled volume used to quantify the area of the cooling pipe holes in the DEMO divertor mock-up. The insert in figure shows the contour limit of each hole area computed by means of 'analyze particles' plugin [22] available for ImageJ software [23].

Table 1. Quantification of the area of each hole detected in the CuCrZr pipe of the DEMO divertor mock-up after failure by HHF load, its error, and results after fitting each hole contour with ellipsoids. In particular, the ellipse aspect ratio and ellipse roundness fitting parameters are provided.

ID number	Area (mm^2)	Error (mm^2)	Ellipse aspect ratio	Roundness
1	0.746	0.019	1.211	0.826
2	0.637	0.019	1.478	0.676
3	2.486	0.019	1.448	0.691

Table 2. Predictions of the coolant flow rate lost through each detected hole in the CuCrZr pipe of the DEMO divertor mock-up.

ID number	Area (mm^2)	Coolant flow rate ($cm^3\ s^{-1}$)	Averaged coolant velocity ($cm\ s^{-1}$)	Coolant flow rate lost through the pipe hole ($cm^3\ s^{-1}$)
1	0.764	116.67	103.16	0.77
2	0.637	116.67	103.16	0.66
3	2.486	116.67	103.16	2.56

5. Conclusions

This pilot experiment has successfully demonstrated the feasibility of using XCT at MeV energy range for non-destructively assessing volumetric defects present in the DEMO divertor mock-up after failure of the component during HHF load at $\sim$8 MWm^{-2} performed at the HIVE facility, UKAEA, United Kingdom. During this test, a loss of cooling on the divertor target was experienced which led to bulk boiling in the pipe-work of some residual coolant and a subsequent expansion of the sample in its central area. The rapid expansion led to a leak of the coolant and rapid migration of some of the inner pipe and interlayer materials to the surface of the W armour. Post-process analysis of CT data has revealed non-destructively the detailed location of the occurred volumetric defects in the component with a spatial resolution of the order of hundreds micrometres. All of these defects were localised in the two central monoblocks of the component. The amount of materials lost by melting of the OFHC copper interlayer and CuCrZr pipe during HHF test was $3143.713 \pm 0.003\ mm^3$ and quantitatively addressed by volumetric analysis on a selected CT sub-volume of the sample closed to the damage. Further, three holes in the cooling pipe has been detected and their area quantified to be 0.746 mm^3, 0.637 mm^3, and 2.486 mm^3, respectively. From the values of the hole area in the CuCrZr pipe we further estimated the flow rate of coolant lost thorough each orifice and of 0.77 $cm^3\ s^{-1}$, 0.66 $cm^3\ s^{-1}$, and 2.56 $cm^3\ s^{-1}$, respectively. A total amount of 4 $cm^3\ s^{-1}$ of coolant lost into the vacuum chamber in the HIVE facility has been predicted.

This experiment has demonstrated for the first time that MeV energy range x-ray tomography could potentially be applied to qualify non-destructively large fusion components despite their large size and inclusion of dense materials such as W. Further, this technology can be used for the inspection of additive manufacturing components where conventional NDE methods might fail, hence opening up more freedom to designers of fusion reactors. Lastly, the image-based nature of MeV

energy range x-ray radiography and tomography results could impact procedures to be followed in the qualification of fusion components for current and future nuclear reactors.

Acknowledgments

This work has received funding from the RCUK Energy Programme (Grant Number EP/I501045) and EPSRC (Grant Number EP/R012091/1). The manufacture of the DEMO divertor mock-up employed in this study as a test-case sample of a relevant fusion component has been realised within the EUROfusion work package 'Divertor' (WPDIV). The authors would like to thanks Dr. Thomas R. Barrett and Dr. Kieran Flinders for the useful discussions, and acknowledge the UK Government Department for Business, Energy and Industrial Strategy for time and resources.

ORCID iDs

Triestino Minniti https://orcid.org/0000-0002-9416-4510

References

[1] Federici G. *et al* 2001 *Nucl. Fusion* **41** 1967–2137
[2] You J.H. *et al* 2018 *Nucl. Mater. Energy* **16** 1–11
[3] You J.H. *et al* 2021 *J. Nucl. Mater.* **544** 152670
[4] Minniti T., Schoofs F., Evans L.M., Kockelmann W., You J.-H. and Lewtas H. 2021 *Fusion Eng. Des.* **169** 112661
[5] You J.H. *et al* 2016 *Fusion Eng. Des.* **109–111** 1598–603
[6] Barrett T.R., McIntosh S.C., Fursdon M., Hancock D., Timmis W., Coleman M., Rieth M. and Reiser J. 2015 *Fusion Eng. Des.* **98–99** 1216–20
[7] Fursdon M. *et al* 2017 *Phys. Scr.* **T170** 014042
[8] Lukenskas A. *et al* 2019 *Fusion Eng. Des.* **146** 1657–60
[9] Minniti T., Watanabe K., Burca G., Pooley D.E. and Kockelmann W. 2018 *Nucl. Instrum. Methods Phys. Res.* A **888** 184–95
[10] Minniti T. *et al* 2016 *J. Instrum.* **11** C03014
[11] Kockelmann W. *et al* 2018 *J. Imaging* **4** 47
[12] Micieli D., Minniti T., Formoso V., Kockelmann W. and Gorini G. 2018 *J. Instrum.* **13** C06006
[13] Micieli D., Minniti T., Evans L.M. and Gorini G. 2019 *Sci. Rep.* **9** 2450
[14] Ramadhan R.S., Kockelmann W., Minniti T., Chen B., Parfitt D., Fitzpatrick M.E. and Tremsin A.S. 2019 *J. Appl. Crystallogr.* **52** 351–68
[15] Minniti T. 2019 *J. Appl. Crystallogr.* **52** 903–9
[16] Evans L.M. *et al* 2018 *Fusion Eng. Des.* **134** 97–108
[17] Flinders K., Bamber R., Lewtas H., Hancock D., Homfray D., Kamalu J. and Barrett T. 2019 *Fusion Eng. Des.* **146** 2040–4
[18] North Star Imaging (https://4nsi.com)
[19] Kak A.C., Slaney M. and Wang G. 2002 *Med. Phys.* **29** 107
[20] Micieli D., Minniti T. and Gorini G. 2019 *SoftwareX* **9** 260–4
[21] *VGSTUDIO MAX Software* (https://volumegraphics.com/en/products/vgsm.html)
[22] Henriques R., Lelek M., Fornasiero E.F., Valtorta F., Zimmer C. and Mhlanga M.M. 2010 *Nat. Methods* **7** 339–40
[23] Schneider C.A., Rasband W.S. and Eliceiri K.W. 2012 *Nat. Methods* **9** 671–5